Molecular Magnets

DOI: 10.1002/ange.201100306

A Spectroscopic Investigation of Magnetic Exchange Between Highly Anisotropic Spin Centers**

Angelika B. Boeer, Anne-Laure Barra, Liviu F. Chibotaru, David Collison, Eric J. L. McInnes, Richard A. Mole, Giovanna G. Simeoni, Grigore A. Timco, Liviu Ungur, Tobias Unruh, and Richard E. P. Winpenny*

Low-dimensional molecular magnets are being studied as potential memory elements for information storage,[1–3] for quantum information processing,[4–6] or as components of molecular machines.[7] One key consideration is the anisotropy of the magnetic centers; this is particularly important for single-molecule magnets[1,8] and single-chain magnets.[9] Modeling magnetic behavior with high anisotropy due to first-order orbital angular momentum is particularly challenging. The most common examples are six-coordinate cobalt(II) complexes, and the slow relaxation seen in some polymetallic cobalt(II) complexes remains controversial.[10] To describe even dimetallic compounds can involve an intimidating level of theory.[11] Here, multi-frequency electron paramagnetic resonance (EPR), inelastic neutron scattering (INS), and magnetic studies are reported, and modern theory is used to generate a simple model. This approach suggests that the exchange in such systems is largely controlled by the orientation of the local magnetic moments.

Dimetallic six-coordinate cobalt(II) compounds are one of the simplest cases in which orbital degeneracy is present in an exchange-coupled system. The synthesis and structures of $[Co_2(H_2O)(O_2CtBu)_4(HO_2CtBu)_4]$ (**1**) and $[Co_2(H_2O)(O_2CtBu)_4(HO_2CtBu)_2(py)_2]$ (**2**; py = pyridine), based on a common $\{Co_2(\mu\text{-}H_2O)(\mu\text{-}O_2CR)_2\}$ core, have been reported.[12] The simplicity of the structures (Figure 1) allows per-deuteration, giving the opportunity for INS studies. Coronado, Güdel, and co-workers have shown how INS can define zero-field level structures and hence exchange-interaction(s).[13–16] However, this contains no information on the highly anisotropic Zeeman interaction(s). This can, in principal, be obtained from EPR, but reports of resolved spectra are very rare.

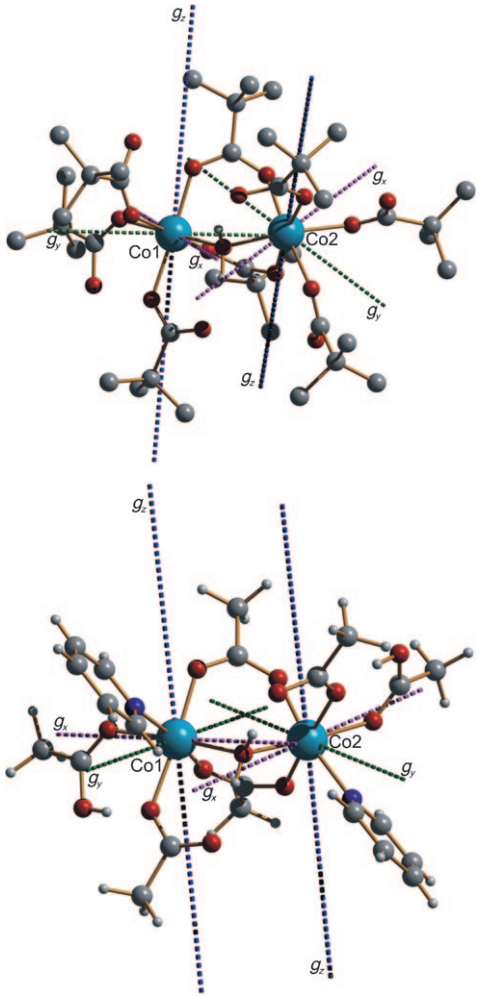

Figure 1. Molecular structures of **1** (top) and **2** (bottom), with principal axes of $\mathbf{g}_i$ for the lowest Kramers doublets of the Co^{II} ions. The length of the vectors is proportional to the magnitude of g_{eff}. Co blue, O red, C gray, N dark blue, H omitted for clarity.

For compound **2** the molar magnetization (M) at 1.8 K increases rapidly with applied magnetic field (H), saturating to 3.75 μ_B (Figure 2). In contrast, compound **1** shows a stepped

[*] Dr. A. B. Boeer, Prof. D. Collison, Prof. E. J. L. McInnes, Dr. G. A. Timco, Prof. R. E. P. Winpenny
School of Chemistry and Photon Science Institute
The University of Manchester, Oxford Road, Manchester (UK)
Fax: (+44) 161-275-4616
E-mail: eric.mcinnes@manchester.ac.uk
Dr. A.-L. Barra
Laboratoire National des Champs Magnétiques Intenses
UPR 3228 CNRS, UJF-INSA-UPS, BP 166
38042 Grenoble Cedex 9 (France)
Prof. L. F. Chibotaru, Dr. L. Ungur
Division of Quantum and Physical Chemistry, University of Leuven
Celestijnenlaan 200F, 3001 Heverlee (Belgium)
Dr. R. A. Mole, Dr. G. G. Simeoni, Dr. T. Unruh
ZWE FRM-II, Lichtenbergstrasse 1, 85747 München (Germany)

[**] This work was supported by the EPSRC (UK), The University of Manchester, the EC NMI3 project, and MAGMANet Network of Excellence. R.E.P.W. holds a Royal Society Wolfson Merit Award.

Supporting information for this article is available on the WWW under http://dx.doi.org/10.1002/anie.201100306.

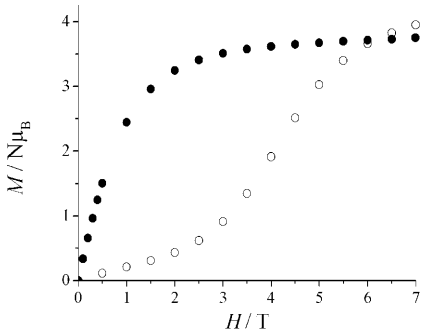

Figure 2. Magnetization (*M*) vs. applied magnetic field (*H*) for polycrystalline samples of **2** (●) and **1** (○) at 1.8 K.

M(*H*) plot, with little magnetization to ca. 2 T before a rapid increase to a similar saturation value (Figure 2). Molar magnetic susceptibility (χ_m) data are similar for **1** and **2** from 300 to 100 K, with a gradual decline in $\chi_m T$. At lower temperatures $\chi_m T$ of **2** reaches a plateau at 4.2 $cm^3 K mol^{-1}$, which is field-dependent below 5 K, while $\chi_m T$ of **1** continues to decline (Figure S1, Supporting Information).

A simple and intuitive approach towards the interpretation of low-temperature data for cobalt(II) ions is the pseudo (or effective) spin-1/2 approximation, where only the lowest-lying Kramers doublet of each ion is considered. The $^4T_{1g}$ ground state (using O_h symmetry labels) is split into six Kramers doublets by the combination of the low-symmetry crystal field and spin–orbit coupling. The lowest doublet is separated by ca. 200 cm^{-1} from the next doublet (see Table S1 for calculated energies); hence, at low temperature, only this doublet is populated. Although this comprises both spin and orbital angular momentum in its wave-function, it can be treated as a pseudo "s_{eff}" = 1/2 state given its two-level nature.

Using this model, the observed low-temperature magnetism has a straightforward possible explanation; in **2** the two $s_{eff} = 1/2$ couple ferromagnetically to give a total effective $S_{eff} = 1$ ground state and an $S_{eff} = 0$ excited state. In **1** the coupling is antiferromagnetic to give an effective singlet ground state. The stepped *M*(*H*) curve for **1** is then due to the crossover of one of the triplet levels with $S_{eff} = 0$ with increasing field. Both the saturation magnetizations for **1** and **2** and the low-temperature plateau in $\chi_m T$ for **2** are consistent with an average $g_{eff} \approx 4$. Note that we can describe the coupled states as $S_{eff} = 0$ and 1 in zero-field, because there are no matrix elements to connect the antisymmetric $2^{-1/2}(|\uparrow\downarrow\rangle - |\downarrow\uparrow\rangle)$ state ($S_{eff} = 0$) with any of the other three states, even for rhombic exchange interactions [giving $2^{-1/2}(|\uparrow\downarrow\rangle + |\downarrow\uparrow\rangle)$ and $2^{-1/2}(|\uparrow\uparrow\rangle \pm |\downarrow\downarrow\rangle)$ "triplet" states]. This is not the case in an applied field (see below).

INS data on per-deuterated samples, $\mathbf{1}^{D}$ and $\mathbf{2}^{D}$, collected in zero-field, are consistent with four-level schemes. Spectra of $\mathbf{1}^{D}$ (6.0 Å neutrons; 0.4 cm^{-1} resolution) between 4 and 16 K show five well-resolved magnetic transitions: three cold bands at 4.7, 9.4, and 11.3 cm^{-1} and two hot bands at 1.9 and 6.6 cm^{-1} (Figures 3, top, and S2). These transition energies give relative energies for the four levels of 0, 4.7, 9.4 and 11.3 cm^{-1} (Figure 3, top inset). The *Q*-dependence[17] (where **Q** is the scattering vector) of the cold transitions are

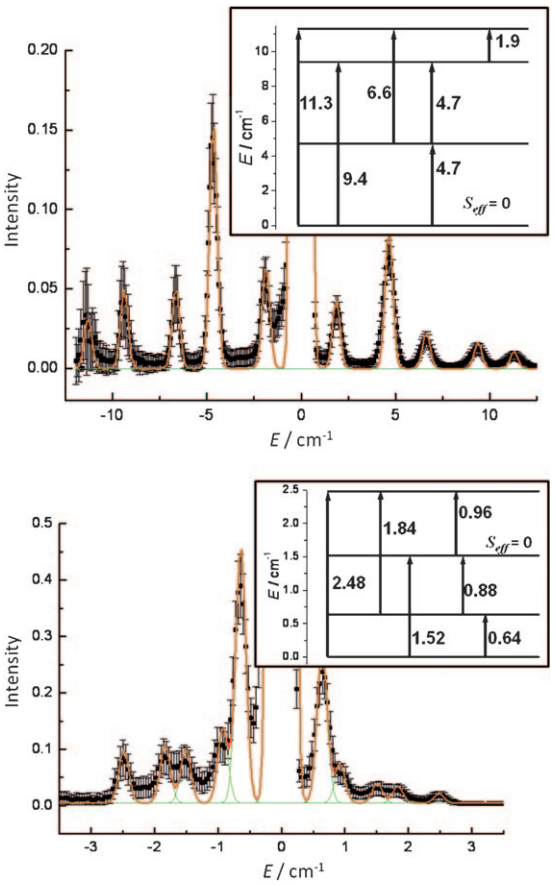

Figure 3. INS spectra of $\mathbf{1}^{D}$, at 16 K with 6.0 Å neutrons (top) and of $\mathbf{2}^{D}$ at 2.4 K with 8.0 Å neutrons (bottom); Gaussian fit to peaks as solid lines. Insets: derived level schemes with possible INS transitions. [Note the model predicts a 0.88 cm^{-1} transition for $\mathbf{2}^{D}$: this would not be resolved from the 0.96 cm^{-1} band within the experimental resolution; both transitions are hot and $\Delta S_{eff} = 1$.]

consistent with $\Delta S_{eff} = 1$ transitions, while those at 1.9 and 6.6 cm^{-1} are consistent with $\Delta S_{eff} = 0$ (Figure S3). This is only possible if the lowest level is the $S_{eff} = 0$ state, consistent with *M*(*H*) data.

A smaller spread of transition energies is observed for $\mathbf{2}^{D}$ under similar conditions (Figure S4, left). A higher resolution (8 Å neutrons; 0.16 cm^{-1} resolution) and lower temperature (0.7 to 16 K) experiment reveals cold transitions at 0.64, 1.52, and 2.48 cm^{-1} and hot transitions at 0.96 and 1.84 cm^{-1} (Figures 3, bottom, and S4, right). This gives relative level energies of 0, 0.64, 1.52, and 2.48 cm^{-1} (Figure 3, bottom inset). The *Q*-dependence of the 0.64, 1.84, and 2.48 cm^{-1} transitions are consistent with $\Delta S_{eff} = 0$ while those at 0.96 and 1.52 cm^{-1} are consistent with $\Delta S_{eff} = 1$ (Figure S5). This is only consistent with the third-highest level (at relative energy 1.52 cm^{-1}) being the $S_{eff} = 0$ state, consistent with the lack of a step in *M*(*H*) data.

In both cases, the data confirm a well-isolated four-level energy manifold arising from coupling of the lowest Kramers doublets of two cobalt(II) ions; experiments up to 60 K at 3.8 Å do not show any further magnetic transitions. The complete lifting of the degeneracy in zero-field implies that

the exchange interactions are rhombic. The smaller spread of transition energies for $\mathbf{2}^{D}$ implies weaker exchange for this compound.

EPR spectra of **1** and **2** at low temperature are well resolved with complicated fine structure. Such resolution is extremely rare for exchange-coupled orbitally degenerate ions,[18–20] and is important because it gives spectroscopic access to the very anisotropic g_{eff}-values. Spectra of **1** are simpler than those of **2** at 94 GHz (Figures 4 and 5); the fewer

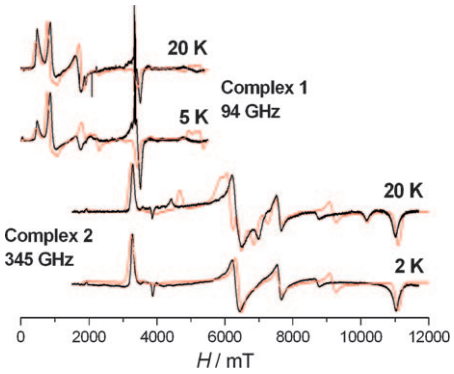

Figure 4. Variable-temperature EPR spectra of polycrystalline samples of **1** at 94 GHz, and **2** at 345 GHz: experimental (black) and calculated (red) with the model in the text. [The sharp $g=2.0$ feature at 94 GHz is due to a Mn^{II} impurity.]

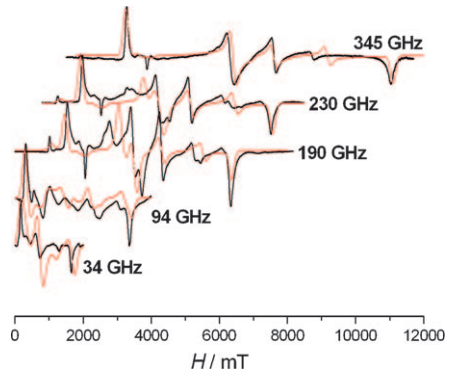

Figure 5. Variable-frequency EPR spectra of polycrystalline sample of **2** at 4 K (2 K at 345 GHz): experimental (black) and calculated spectra (red) with the model described in the text.

transitions are consistent with a larger exchange interaction. Higher-frequency spectra, up to 345 GHz, have been measured for **2** and reveal up to twelve transitions covering the full magnetic field range (Figure 5).

We have modeled the EPR spectra using the simple spin-Hamiltonian (1):

$$\hat{\mathbf{H}} = \hat{\mathbf{s}}_1 \cdot \mathbf{J} \cdot \hat{\mathbf{s}}_2 + \mu_B \sum_{i=1,2} \mathbf{H} \cdot \mathbf{g}_i \cdot \hat{\mathbf{s}}_i \qquad (1)$$

where $\mathbf{g}_i$ are the effective **g**-matrices for the $s_{\mathrm{eff}}=1/2$ centers. Note we define a single anisotropic exchange matrix, **J**, rather than separate isotropic and anisotropic components. There are many variables since **J** and $\mathbf{g}_i$ are expected to be highly anisotropic and there is no requirement for these interaction matrices to share axes. To avoid over-parameterization we have fixed many parameters from INS and ab initio calculations.

The principal values of **J** are fixed such that diagonalization of Equation (1) gives the zero-field energies determined from INS. This gives $J_{x,y,z}=+2.8, +6.6, +16.0\ \mathrm{cm}^{-1}$ for **1** and $J_{x,y,z}=+0.32, +1.60, -3.36\ \mathrm{cm}^{-1}$ for **2**. [We use *xyz* to label local principal axes of the matrices/tensors in Equation (1) and *XYZ* to label a common molecular coordinate frame.] The sign of the largest component is fixed as antiferromagnetic or ferromagnetic, respectively, as observed from $M(H)$, and the signs of $J_{x,y}$ as necessary to justify the pattern of hot and cold bands and their Q-dependence in INS. Note that $J_{x,y}$ are positive while J_z is negative for **2**: this gives the $S_{eff}=0$ state as the third level in zero field.

We have calculated the principal axes and orientations of $\mathbf{g}_i$ by ab initio methods, based on the crystal structures, using methods described elsewhere[21] (Table S1). The calculated signs of the product of the $\mathbf{g}_i$ principal values were positive for both **1** and **2**. Hence, we can take all of them with positive signs; a detailed discussion will be given elsewhere (negative g values have been used to model powder magnetic data in a recent study of a $(Co^{II})_5$ complex[22]). The calculated $\mathbf{g}_i$ are highly rhombic ($g_{x,y,z}\approx 2, 4, 7$; Table S1) but within the range expected for rhombically distorted six-coordinate Co^{II}.[23] For **2** the two g_z are near co-parallel (14° or, equivalently, 166°; Table S3) to each other and are near perpendicular (80°) to the Co-O-Co plane (Figure 1). For **1** the two g_z make a much greater angle to each other (38°; Table S2) and to the Co-O-Co plane (61 and 76° for the two independent Co ions; Figure 1).

The two Co^{II} ions in **2**, and hence $\mathbf{g}_{Co1}$ and $\mathbf{g}_{Co2}$, are symmetry-equivalent, being related by a crystallographic two-fold axis bisecting the Co-O-Co angle.[12] From symmetry arguments, one of the principal axes of **J** must be coincident with this two-fold axis (we choose this as Y). The remaining two axes of **J** can be located anywhere in the plane normal to the C_2 axis. Single-crystal magnetic studies on **2** give the location of two of the crystal magnetic axes as parallel (X) and perpendicular (Z) to the Co–Co vector. In order to avoid over-parameterization, we have taken these as the remaining two principal axes of **J**. This choice is convenient, because it makes $\mathbf{g}_{Co1}$ and $\mathbf{g}_{Co2}$ symmetry-related about **J**, which can then be used to define the *XYZ* molecular frame. Although **1** has only pseudo two-fold symmetry, we have kept the same molecular frame and have imposed $\mathbf{g}_{Co1}=\mathbf{g}_{Co2}$.

In our initial EPR calculations we fixed both the orientations and values of $\mathbf{g}_i$, and then cycled through the possible assignments of the principal values of **J** to $J_{X,Y,Z}$ (and also through the possible sign combinations in order to test the INS assignments). In each case, only one combination gave reasonable results compared to the experimental data. For these solutions we refined the principal g_{eff}-values. For **1** we found good simulations (Figure 4) with $J_{X,Y,Z}=+6.6, +2.8, +16.0\ \mathrm{cm}^{-1}$ and $g_{x,y,z}=2.4, 4.0, 7.0$. For **2** we get $J_{X,Y,Z}=+1.60, +0.32, -3.36\ \mathrm{cm}^{-1}$ and $g_{x,y,z}=2.3, 3.9, 6.2$ (Figure 4 and Figure 5). The simulations are remarkably good (including temperature dependence, Figure 4) given the

simplicity of the model and the extreme sensitivity to the parameters, e.g., to the orientations of $\mathbf{g}_i$. Importantly, they reproduce the spread of the spectra of **2** over a wide frequency and field range (Figure 5).

The four levels can be described as $S_{\text{eff}} = 0$ and 1 in zero applied field (see above). For **2**, the assignment of the third level as the singlet (Figure 3) is confirmed by the EPR results. It is only possible to model the variable-temperature effects in the high-frequency spectra (e.g., the highest-field "doublet" centered on 10.6 T at 345 GHz, Figure 4) using the sign combination of $J_{X,Y,Z}$ given above. The consistency with INS gives confidence in the model. However, in an applied field the huge *g*-anisotropies—and the non-colinearity of the axes—lead to extensive mixing of the four states. For example, a Zeeman diagram for **2** with the magnetic field at an angle $\phi = 40°$ in the *XY* plane ($\theta = 90°$) shows all four levels evolving with field, with allowed EPR transitions between levels 1→2 and 3→4 at high field (see Figure 6 with 345 GHz transitions shown; these give rise to the highest-field "doublet" in Figure 4). A simple parameterization as $S_{\text{eff}} = 0$ and 1 is not possible in applied field.

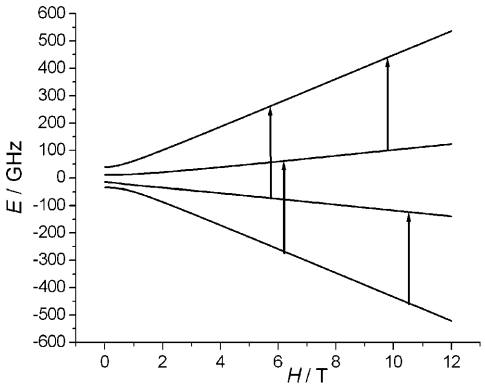

Figure 6. Zeeman diagram for **2** with applied magnetic field at an angle of $\phi = 40°$, $\theta = 90°$ (in the *XY* plane) with allowed 345 GHz EPR transitions.

In summary, we are able to interpret the high-quality INS and EPR data for **1** and **2**, giving detailed information on the exchange and $\mathbf{g}_i$ matrices. Both are highly rhombic and their relative orientations appear to be related. Magnetostructural correlations typically look at structural parameters associated with the superexchange pathways. Here the key parameter might be the angle at the bridging water molecule. In **1** and **2** this is 110° and 108°, respectively. We have studied five further compounds (differing only in terminal ligands from **1** and **2**); all have larger Co-O-Co angles and in each case the magnetic behavior is similar to that of **1**. However, it seems surprising that such a small change in angle should have such a significant influence.

Instead, a possible correlation arises from the orientations of the local magnetic moments, as reflected in the $\mathbf{g}_i$ axes, with respect to the superexchange path. In both **1** and **2**, the dominant component of the exchange (J_z, determining the overall sign of the interaction) is perpendicular to the Co-O-Co plane (i.e. along *Z*). In **2** the two largest g_{eff} values (g_z) lie near normal (80°) to this plane; in **1** they are significantly further skewed from this plane (average 68°). We have performed ab initio calculations for two further complexes, and found angles of 45–70°; in both cases the exchange is also antiferromagnetic from magnetization studies.

This suggests that the relationship between the local crystal field about the cobalt centers and the superexchange pathway is controlling the magnetic interaction. Others have noted the importance of the orientation of $\mathbf{g}_i$ in interpreting magnetic data of polymetallic Co^{II} complexes.[22] In a sense, this is analogous to magnetostructural correlations for spin-only ions such as copper(II), where the crystal field directions are easily established by inspection. For Co^{II}, the local crystal field can vary subtly with minor changes in ligand sphere, and this could explain the diverse magnetism displayed by polymetallic cobalt cages and single-chain magnets.[24] Similar considerations must apply to other highly anisotropic spin centers such as 4f ions.[25,26]

Experimental Section

INS spectra were measured on a multi-chopper time-of-flight instrument[27] TOFTOF at FRM-II of the Technische Universität München: data were normalized to a vanadium sample and background-subtracted using an empty can. 34 and 94 GHz EPR spectra were measured on Bruker instrumentation at the EPSRC National EPR Facility at Manchester. High-frequency/field EPR spectra were measured at the LNCMI-CNRS at Grenoble on a home-built spectrometer. Simulations used Stoll's EasySpin.[28]

Received: January 13, 2011
Published online: March 29, 2011

Keywords: cluster compounds · cobalt · EPR spectroscopy · inelastic neutron scattering · magnetic properties

[1] R. Sessoli, D. Gatteschi, A. Caneschi, M. A. Novak, *Nature* **1993**, *365*, 141–143.
[2] P. Gambardella, S. Stepanow, A. Dimitriev, J. Honolka, F. M. F. de Groot, M. Lingenfelder, S. S. Gupta, D. D. Sarma, P. Bencok, S. Stefanescu, S. Clair, S. Pons, N. Lin, A. P. Seitsonen, H. Bune, J. V. Barth, K. Kern, *Nat. Mater.* **2009**, *8*, 189–193.
[3] M. Mannini, F. Pineider, C. Danieli, F. Totti, L. Sorace, P. Sainctavit, M.-A. Arrio, E. Otero, L. Joly, J. C. Cezar, A. Cornia, R. Sessoli, *Nature* **2010**, *468*, 417–421.
[4] M. N. Leuenberger, D. Loss, *Nature* **2001**, *410*, 789–793.
[5] S. Bertaina, S. Gambarelli, T. Mtira, B. Tsukerblatt, A. Müller, B. Barbara, *Nature* **2008**, *453*, 203–207.
[6] G. A. Timco, S. Caretta, F. Troiani, R. J. Pritchard, E. J. L. McInnes, A. Ghirri, A. Candini, P. Santini, G. Amoretti, M. Affronte, R. E. P. Winpenny, *Nat. Nanotechnol.* **2009**, *4*, 173–178.
[7] C.-F. Lee, D. A. Leigh, R. G. Pritchard, D. Schultz, S. J. Teat, G. A. Timco, R. E. P. Winpenny, *Nature* **2009**, *458*, 314–318.
[8] G. Aromí, E. K. Brechin, *Struct. Bonding (Berlin)* **2006**, *122*, 1–68.
[9] C. Coulon, H. Miyasaka, R. Clérac, *Struct. Bonding (Berlin)* **2006**, *122*, 163–206.
[10] M. Murrie, *Chem. Soc. Rev.* **2010**, *39*, 1986–1995.
[11] A. Palii, B. Tsukerblatt, J. M. Clemente-Juan, E. Coronado, *Int. Rev. Phys. Chem.* **2010**, *29*, 135–230.

[12] G. Aromí, A. R. Bell, M. Helliwell, J. Raftery, S. J. Teat, G. A. Timco, O. Roubeau, R. E. P. Winpenny, *Chem. Eur. J.* **2003**, *9*, 5142 – 5161.
[13] H. Andres, J. M. Clemente-Juan, M. Aebersold, H.-U. Güdel, E. Coronado, H. Büttner, G. Kearly, J. Melero, R. Burriel, *J. Am. Chem. Soc.* **1999**, *121*, 10028 – 10034.
[14] J. M. Clemente-Juan, E. Coronado, A. Gaita-Ariño, C. Giménez-Saiz, G. Chaboussant, H.-U. Güdel, R. Burriel, H. Mutka, *Chem. Eur. J.* **2002**, *8*, 5701 – 5708.
[15] J. M. Clemente-Juan, E. Coronado, A. Gaita-Ariño, C. Giménez-Saiz, H.-U. Güdel, A. Sieber, R. Bircher, H. Mutka, *Inorg. Chem.* **2005**, *44*, 3389 – 3395.
[16] H. Andres, J. M. Clemente-Juan, R. Basler, M. Aebersold, H.-U. Güdel, J. J. Borrás-Almenar, E. Coronado, H. Büttner, S. Janssen, *Inorg. Chem.* **2001**, *40*, 1943 – 1950.
[17] A. Furrer, H. U. Güdel, *Phys. Rev. Lett.* **1977**, *39*, 657 – 660.
[18] J. Liu, S. Datta, E. Bolin, J. Lawrence, C. C. Beedle, E-C. Yang, P. Goy, D. N. Hendrickson, S. Hill, *Polyhedron* **2009**, *28*, 1922 – 1926.
[19] Y. Nakagawa, T. Kashiwagi, H. Yamaguchi, S. Kimura, Z. Honda, K. Yamada, K. Kindo, M. Hagiwara, *J. Phys. Soc. Jpn.* **2006**, *75*, 124708.
[20] A. Figuerola, V. Tangoulis, Y. Sanakis, *Chem. Phys.* **2007**, *334*, 204 – 215.
[21] L. Ungur, W. van den Heuvel, L. F. Chibotaru, *New J. Chem.* **2009**, *33*, 1224 – 1230, and references therein.
[22] F. Klöwer, Y. Lan, J. Nehrkorn, O. Waldmann, C. E. Anson, A. K. Powell, *Chem. Eur. J.* **2009**, *15*, 7413 – 7422.
[23] L. L. Lohr, J. C. Miller, R. R. Sharp, *J. Chem. Phys.* **1999**, *111*, 10148 – 10158.
[24] A. Caneschi, D. Gatteschi, N. Lalioti, C. Sangregorio, R. Sessoli, G. Venturi, A. Vindigni, A. Rettori, M. G. Pini, M. A. Novak, *Angew. Chem.* **2001**, *113*, 1810 – 1813; *Angew. Chem. Int. Ed.* **2001**, *40*, 1760 – 1763.
[25] J. Luzon, K. Bernot, I. J. Hewitt, C. E. Anson, A. K. Powell, R. Sessoli, *Phys. Rev. Lett.* **2008**, *100*, 247205.
[26] L. F. Chibotaru, A. Soncini, *Angew. Chem.* **2008**, *120*, 4194 – 4197; *Angew. Chem. Int. Ed.* **2008**, *47*, 4126 – 4129.
[27] T. Unruh, J. Neuhaus, W. Petry, *Nucl. Instrum. Methods Phys. Res. Sect. A* **2007**, *580*, 1414 – 1422.
[28] S. Stoll, A. Schweiger, *J. Magn. Reson.* **2006**, *178*, 42 – 55.

